



Near-surface structure of the Carpathian Foredeep marginal zone in the Roztocze Hills area

M. Majdański¹ · J. Grzyb¹ · B. Owoc¹ · T. Krogulec² · A. Wysocka²

Received: 27 October 2017 / Accepted: 22 March 2018 / Published online: 29 March 2018
© The Author(s) 2018

Abstract

Shallow seismic survey was made along 1280 m profile in the marginal zone of the Carpathian Foredeep. Measurements performed with standalone wireless stations and especially designed accelerated weight drop system resulted in high fold (up to 60), long offset seismic data. The acquisition has been designed to gather both high-resolution reflection and wide-angle refraction data at long offsets. Seismic processing has been realised separately in two paths with focus on the shallow and deep structures. Data processing for the shallow part combines the travel time tomography and the wide angle reflection imaging. This difficult analysis shows that a careful manual front mute combined with correct statics leads to detailed recognition of structures between 30 and 200 m. For those depths, we recognised several SW dipping tectonic displacements and a main fault zone that probably is the main fault limiting the Roztocze Hills area, and at the same time constitutes the border of the Carpathian Forebulge. The deep interpretation clearly shows a NE dipping evaporate layer at a depth of about 500–700 m. We also show limitations of our survey that leads to unclear recognition of the first 30 m, concluding with the need of joint interpretation with other geophysical methods.

Keywords Carpathian Foredeep · Seismic imaging · Traveltime tomography · Near-surface · Joint seismic interpretation

Introduction

The reflection seismic methods are well known and successfully used in industrial applications over the decades. They are also more often used in smaller scales to recognize near-surface structures. The potential of high-resolution seismic reflection methods has been proven by number of groups studding unconsolidated or postglacial sediments (Buker et al. 1998; Bachrach and Nur 1998; Steeples and Miller 1998; Francese et al. 2007). Standard reflection methods can resolve structures starting from several meters down to several hundreds of meters (Pullan and Hunter 1990; Steeples and Miller 1990; Feroci et al. 2000; Steeples 2000; Dusar et al. 2001; Sugiyama et al. 2003; Bruno et al. 2010; Green et al. 2010).

To recognize the near-surface geological structures an optimal solution is to utilise wide-angle observation and combine them with high resolution reflection data. A successful applications of this approach (Bruno et al. 2010, 2013) shows, that seismic velocities recognized from observed refractions significantly enhance the reflection image of shallow structures.

Here, we report the result of joint interpretation of wide-angle seismic along 2D profile designed to recognize the structure of the marginal zone of the Carpathian Forefront. Recorded large offsets were helpful not only to estimate velocities, but also to image a deep bedrock reflection, that would not be possible using standard deployment. Moreover, designed survey with wireless stations and especially designed accelerated weight drop source was cost-effective and can be performed in a very short time giving a productive tool for the geological studies. Combination of reflection seismic imaging and travel time tomography, that is the tool to recover a high resolution images, has been used before in tectonic scale (Malinowski et al. 2013), the industrial scale (Majdański et al. 2016; Vesnaver et al.

✉ M. Majdański
mmajd@igf.edu.pl

¹ Institute of Geophysics, Polish Academy of Sciences, ks. Janusza 64, 01-452 Warsaw, Poland

² Faculty of Geology, University of Warsaw, Żwirki i Wigury 93, 02-089 Warsaw, Poland

1999), but also in near-surface studies (Bruno et al. 2010, 2013).

Geological setting

The present-day area of the Roztocze Hills constitutes as a narrow range of hills, stretching from north-west to south-east from Kraśnik in Poland to Lviv in Ukraine. The area divides the eastern part of the Sandomierz Basin from the Lublin Upland and the Pobuża Basin (Konracki 1994). The area where the measurements were made is located on the Roztocze Hills along the Carpathian Foredeep marginal zone (Fig. 1). During the Neogene (Miocene) time, this area belonged to the north-eastern part of the outer ramp of the Carpathian Foreland Basin (Wysocka 2006) and it is recognized as their forebulge (Jankowski and Margielewski 2015; Wysocka et al. 2016).

This region is dominated on the surface by sedimentary rocks, mainly Cretaceous marls or sandstones and Neogene (Miocene) sandstones, limestones and marls. These rocks were formed in shallow sea with high hydrodynamic energy.

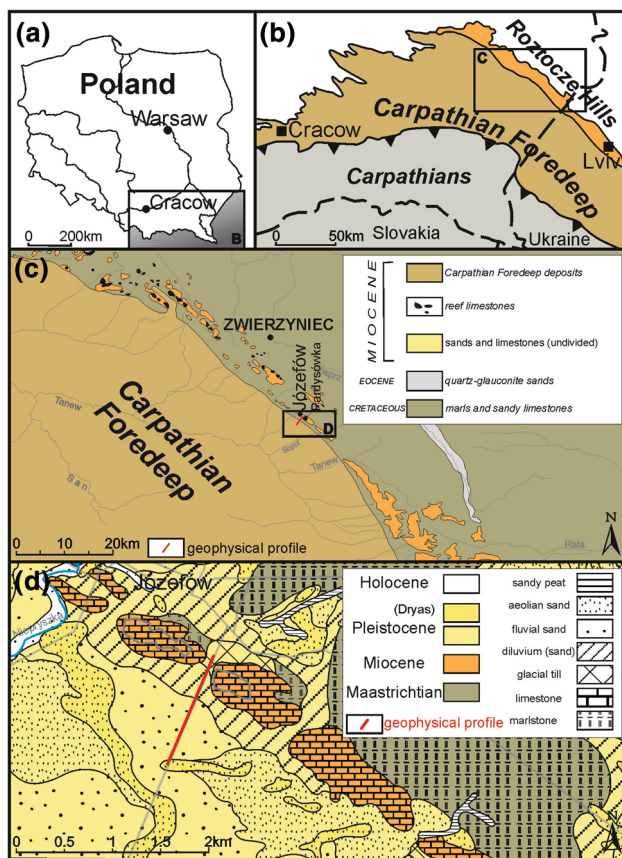


Fig. 1 Schematic map showing: **a** general location of the study region in Poland, **b** tectonic structures in the area; **c** location of seismic profile in the marginal zone of the Carpathian Foredeep; **d** detailed geological map in the vicinity of the profile (after Kurkowski 1998)

Miocene rocks are preserved only in the form of erosional patches along south-western marginal zone (Wysocka and Jasionowski 2006). Carpathian Foredeep in the north eastern part consists mostly of Miocene flat bedded lightly lithified shales, of the same age as the rocks described above, covered by thin layer of Quaternary sediments. In the whole Miocene sequence, the only one characteristic layer, evaporates, consists mainly of anhydrites and gypsum. This layer has variable thickness from 0 up to 60 m and has great significance as the main correlation level and seismic marker on the scale of the entire Carpathian Foredeep (Myśliwiec 2004; Krzywicz 2001). These beds can be observed in the Kozaki 1 drill core. Drilling was done approximately 7.5 km to the south-west from the beginning of the profile. These evaporates are mainly gypsum with a thickness of 34 m and occurs at a depth of 609–643 m. This salina basin was developed during the Badenian salinity crisis in northern Central Paratethys (Bąbel 2004).

Due to the difficulty of stratigraphic recognition of sedimentary rocks on the area of the Roztocze Hills, evaporate layer is the only certain horizon which allowed to determine the relative age of the succession. The lack of evaporates layer on the Polish part of the Roztocze Hills area and different types of rocks with different thicknesses are the main problems in the deposits correlation along the north-eastern Carpathian Foredeep marginal zone.

Measurements were made between Józefów and Parzyszawka quarries, which are located in the distance of about 950 m from each other, on the most south-western range of hills of the Roztocze Hills area. Both of them are characterized by Miocene complex, consisting mainly of conglomerates and limestones (Wysocka et al. 2006). The whole complex is located directly on the Cretaceous basement and is inclined slightly toward the south (Roniewicz and Wysocka 1999). In both quarries many normal and reverse faults were found, associated with post-sedimentary Miocene or younger seismic activity in the area. Their planes are parallel to the Carpathian Foredeep marginal zone (Jaroszewski 1977; Jankowski and Margielewski 2015). All observed faults are crossing all the layers at a low angle (Wysocka et al. 2006).

The seismic survey and the field works

The measurements were performed during 3 days in May 2017 along the forest road near Józefów in the Roztocze Hills area, in a direction that crosses the studied structures perpendicularly. For seismic recording we used 60 standalone DATA-CUBE stations with GPS timing connected to 4.5 Hz vertical geophones. As a seismic source we used modified PEG-40 accelerated weight drop with designed handcart equipped with electric power generator. This

autonomous system can be operated by two man in rough terrain, and gives reliable and repeatable seismic signals in efficient way. Additionally, the source was equipped with time measurement system based on GPS time, that stored in laptop the time of each stroke based on closure of the electric circuit. The timing system has precision of 1 ms. The whole production was divided for four deployments (Fig. 2) resulting in the total length of 1280 m. Both sources and receiver spacing was 5 m, and for each deployment additional 10 shots to each side was performed resulting in the fold spanning from 22 to 60. The profile was crossing the hill, resulting in complicated elevation along it, especially changing for the last deployment. The total difference in elevation was 22 m. For each shot position, four strokes has been measured to maximise signal to noise ratio. Those records were further stacked using diversity stack technique. An example of raw shot gathers are presented in left panel of Figs. 3 and 4a. A maximum energy in recorded signals is visible around 30 Hz with lower frequencies strictly connected with surface waves. All survey parameters are summarised in Table 1.

Data processing

Reflection seismic imaging

The data were processed using a simple but effective operations that are summarised in Table 2.

The processing has been performed separately for shallow area and for deep structures. For both paths the continuously recorded data has to be cut according to shot times. The next step was to add geometry and sort to shot gathers with detailed quality check. This step is time consuming but important in case of wireless stations, as mistakes in geometry are easy to make and might have a severe impact on the final quality. Further on, a trace editing was performed to exclude noisy channels resulted from poor geophone coupling. Elevation statics was estimated based on the topography and the floating datum has been set just below the lowest elevation at 240 m. Refraction statics was calculated using standard routines implemented in the commercial seismic software with limited offset of 100 m. This allows to recognize the weathering layer without taking into account large velocity variations resulted from change of topography. A next step in common processing was careful front mute to remove guided waves and preserve wide angle shallow reflections. This procedure is crucial, as explained in many papers (Buker et al. 1998; Robertsson et al. 1996), and has been manually performed for each shot. The effect of application of front mute is presented in Fig. 3 in middle panels, where clearly refracted arrivals have been removed while shallow reflections are preserved. The first recognition of near-surface velocities based on analysis of shallow reflections flattening shows variable velocities along the profile that varies between 1400 and 1600 m/s. The effect of reflection flattening is present in Fig. 3 (right panels),

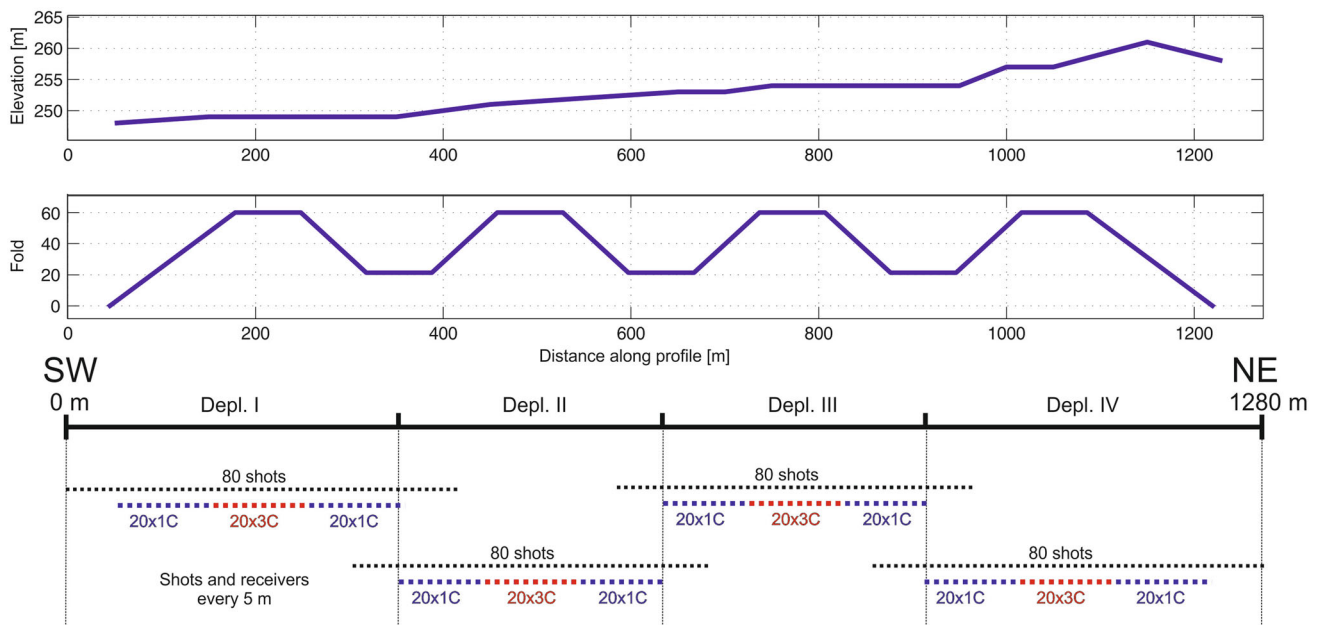


Fig. 2 Field measurement scheme showing four deployments (bottom) using 60 seismic stations and 80 shot positions in each. Thanks to overlaps of shots, the minimum fold was set as 22 (middle panel).

The top panel shows the significant change of 22 m in the elevation along 1280 m long profile

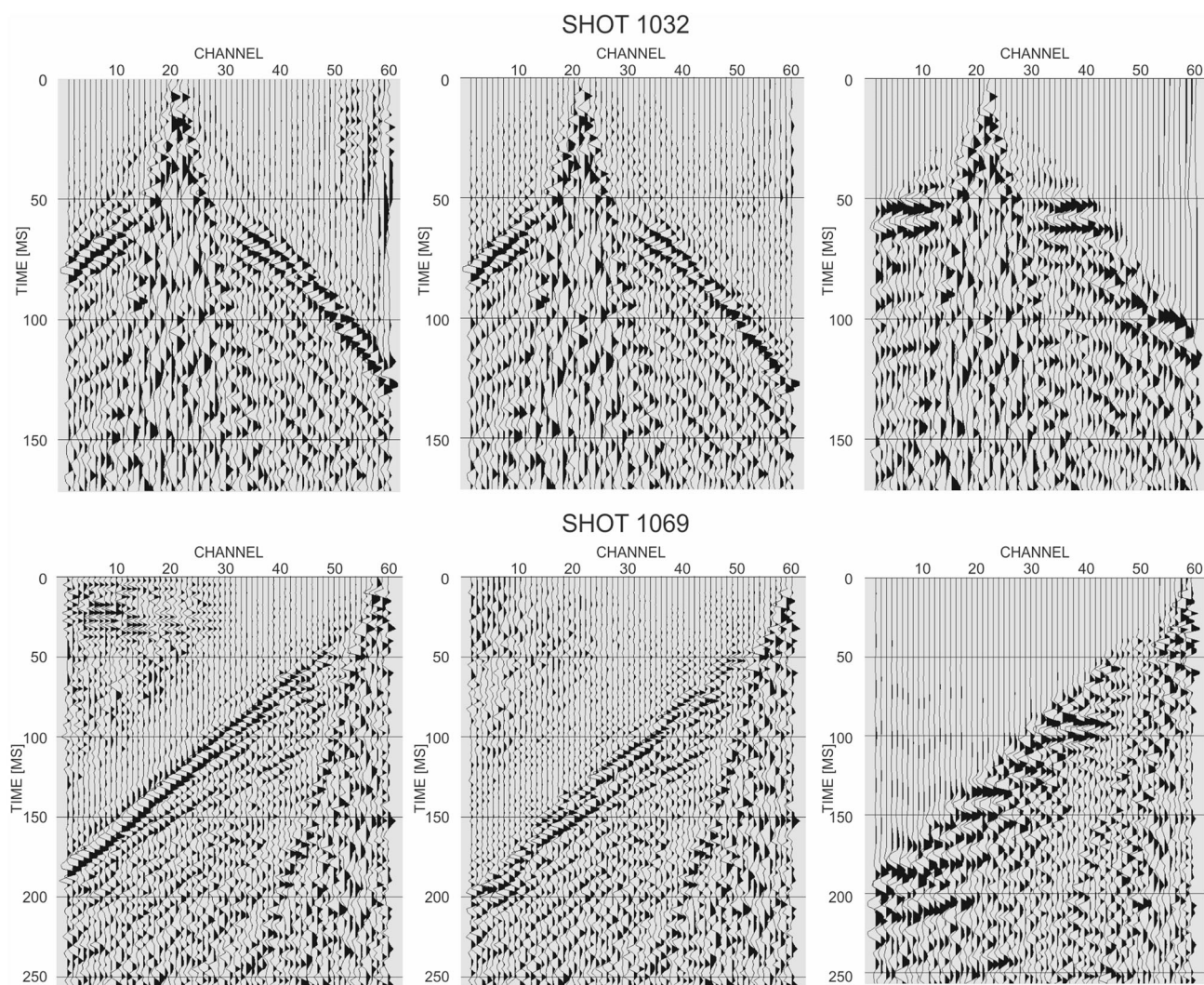


Fig. 3 Example of shot gathers for shots 1032 and 1069 (left panels) after diversity stack of four repeated weight drops. The middle panels show carefully selected front mute, that removes linear refraction arrivals. Right panels show the NMO effect with velocity of 1600 and

1400 m/s, respectively. Clear shallow reflections are visible at 55 ms for shot 1032, and 90 and 140 ms for shot 1069. All panels presented with AGC (100 ms) applied

showing also effect of optimal combination of 70% stretch mute and the front mute.

One of the problems in near-surface processing are strong amplitudes of surface waves that covers useful wide-angle reflections. In our case a simple high-pass filter was efficient enough to attenuate most of surface waves. The best results were obtained when filtering above 30 Hz as presented in Fig. 4c, d. Moreover, high-pass filter attenuates also long wavelength characteristics in shot gathers. Figure 4 shows also a spectral content for an example shot gather showing significant reduction of amplitudes with frequency. To recover sharp images we used spectral whitening technique that is strengthening high frequencies (see Fig. 4d). For this step several deconvolution techniques has been tested, including predictive deconvolutions

and spectral whitening. Figure 5 shows an example results using surface consistent deconvolution, surface consistent spectral whitening, single trace deconvolution and spectral whitening. Choosing an optimal deconvolution we were looking for a sharp and coherent wide-angle reflections, like the one at 120 ms, and one at 270 ms. Both surface consistent approaches (Fig. 5a, b) result in poor enhance of high frequencies, thus smeared reflections. Although, the deconvolution performed for each trace separately results in the flattest spectrum (Fig. 5c) wide-angle reflections are not coherent. Finally, we decided to use spectral whitening in range of 10–180 Hz (Fig. 5d) because it gives the clearest image.

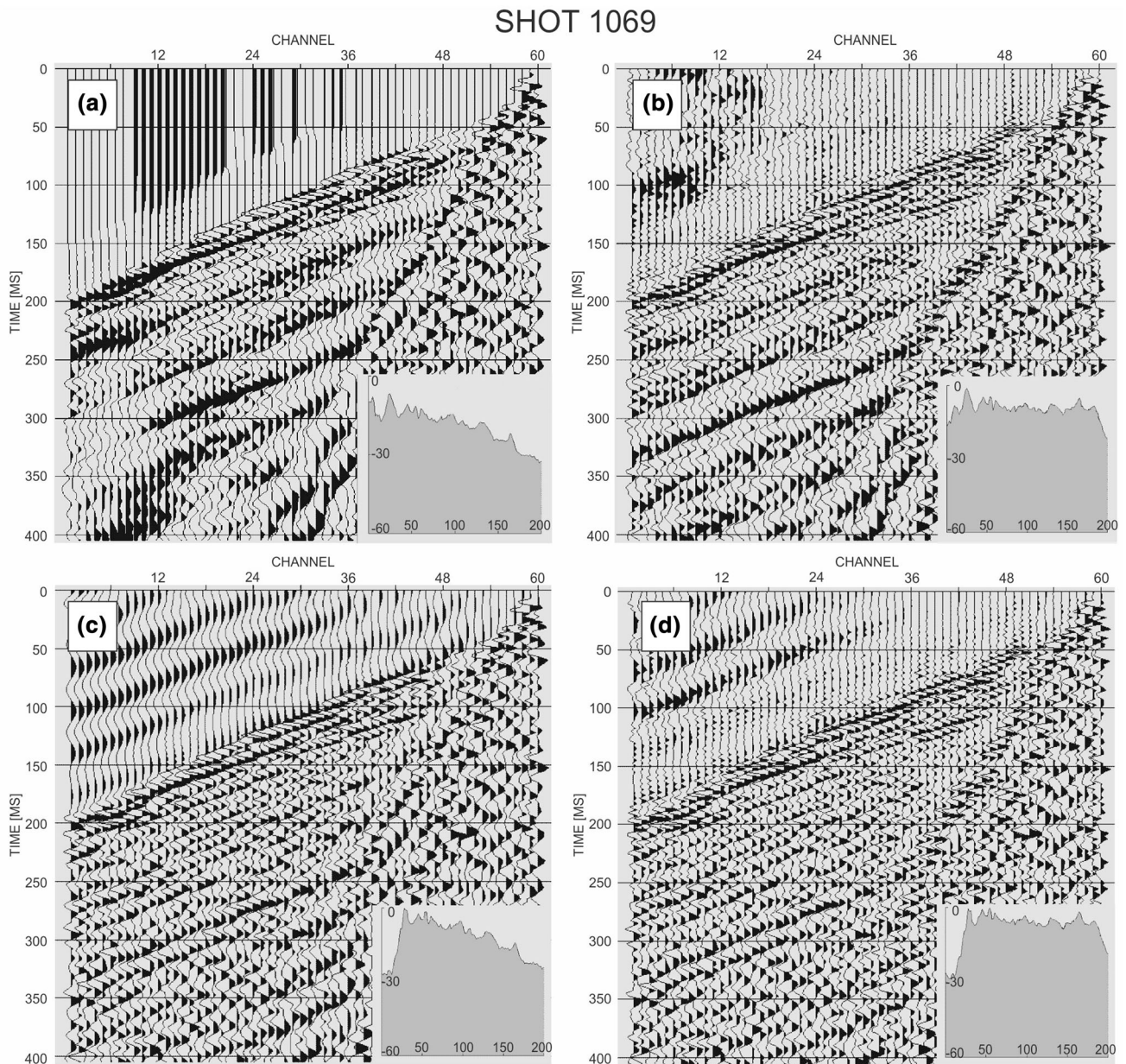


Fig. 4 Example of optimal processing for shot 1069. Raw gather after diversity stack of four repeated weight drops **(a)**; gather after spectral whitening **(b)** shows flat spectrum up to the 180 Hz; **(c)**, **(d)** shows corresponding processing steps as in **(a)**, **(b)** with applied high pass filter

above 30 Hz; inlets in each panel shows spectral content of the gather. All panels presented with AGC (100 ms) and front mute applied

The shallow structure processing

Having problems with standard semblance velocity analysis we wanted to recognize the velocity structure in the shallow part using other techniques. For that, we used well known travel time tomography. The first breaks were manually picked for every fifth shot resulting in 52 regularly spaced shots along the whole profile. All receivers were used in this procedure giving offsets from 5 to 360 m. The refraction arrivals were clearly visible at all offsets,

but after careful elimination of noisy channels we prepared the set of 2600 travel times. This travel time set has been inverted using JIVE3D software (Hobro 1999) for a smooth velocity model with defined topography. The inversion procedure was performed according to standard scheme (Majdański et al. 2016; Zelt 1999) resulting in an interesting velocity distribution presented in Fig. 6. The velocity structure is rather smooth with strong increasing gradient with depth, but also with an increasing trend toward NE. Around CDP 480 a strong gradient marks

Table 1 Acquisition parameters

Feature	Measurement
Vertical stack	4
Sampling interval	2.5 ms
Record length	1 s
Receivers	4.5 Hz
Station interval	5 m
Shot interval	5 m
Active channels	60
Fold	22–60
Offset	0–345 m

sudden change of velocity that indicate a SW dipping fault. Three other smaller gradients indicate discontinuity of velocity with more horizontal SW dipping direction. To verify reliability of tomographic result, a middle panel of Fig. 6 shows ray paths from the last iteration of inversion. It proves that all mentioned observations are in well covered areas. This verified result for the first 60 m is alternative information that was further used to create correct velocity field for reflection imaging. With this additional information it was possible to perform semblance based velocity analysis for observed shallow reflections down to 200 ms. All shallow velocities has been further tested by NMO application on shot gathers along the profile. Flattening of wide-angle reflections (see example Fig. 3) confirming that those shallow velocities are correct. The final velocity model in depth domain is presented in the lower panel of Fig. 6. It was generated as a simple extrapolation of tomographic velocities in shallow areas for large depths.

The shallow processing includes both elevation and refraction static corrections and careful front mute.

Spectral whitening has been applied to eliminate spectral differences between shots and effect of variable coupling of receivers. For NMO correction we used velocity model from Fig. 6. After the stacking procedure resulting section was FK filtered (with velocity of 50 m/s) and depth converted using the same velocity field. The final stack in depth domain is presented in Fig. 7 (top). Looking closely at the first 200 m we observe several flat reflections spanning from the beginning of the profile till CDP 450. Unfortunately there are no borehole information to verify and classify those reflections. A sudden change of reflectivity is observed at CDP 460 where the fault exist and is confirmed at the surface as a morphological edge. This is probably the main fault limiting the Roztocze Hills area from the south west, and at the same time constitutes the border of the Carpathian Forebulge. At CDP 460–500 there is an area of low reflectivity (yellow polygon in Fig. 7) that coincides with strong velocity gradient in tomography. In this area some discontinuities in small reflectivity is visible (marked with black dashed line). The flat reflections on a left side show small discontinuities that could be traced to form lines gently dipping in SW direction. They could be interpreted as small tectonic displacements that do not reach the surface. Three of those structures (solid yellow lines) are confirmed in tomographic result (lower panel in Fig. 7) by areas of dipping velocity gradients. Unreliable tomographic results are greyed out, so we can confirm internal faults at CDP 120, 210, 310 and 410. The other discontinuities are not that sharp in the seismic image and are marked with dashed lines.

The deep structure processing

In the deep structure processing path, two additional steps were needed to enhance energy at larger times. Firstly, we used spherical divergence procedure linearly dependent on

Table 2 Two paths of data processing

	Common processing	Deep focus (additional steps)
1	Data cutting	
2	Geometry and sorting	
3	Trace editing	
4	Elevation statics	
5	Refraction statics	
6	Front mute	
7		Spherical divergence with time
8	Spectral whitening (10–180 Hz)	
9		Tail mute
10	NMO	
11	Stack	
12	FK and high-pass filtering	
13	Depth conversion	

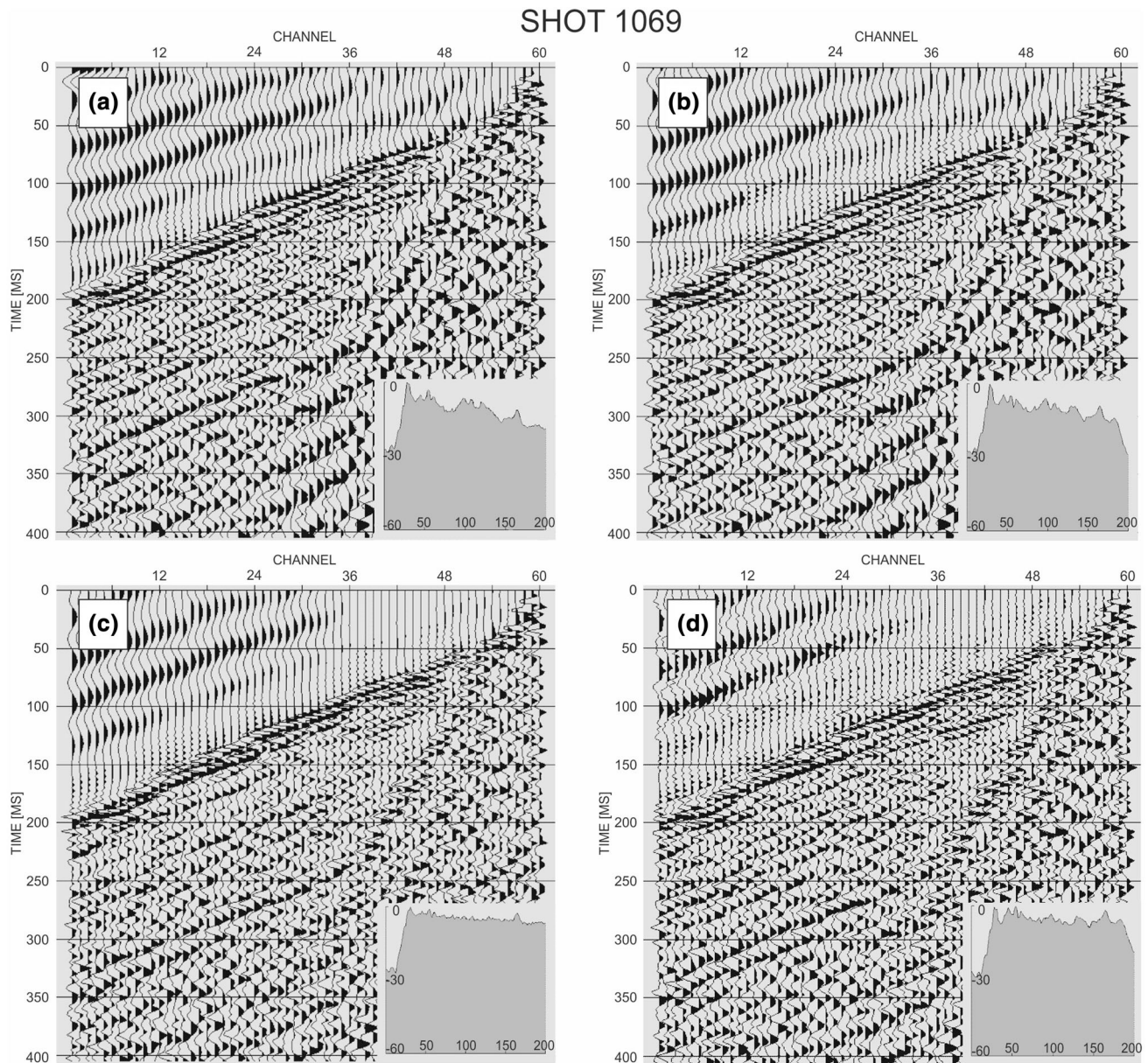


Fig. 5 Example shot 1069 deconvolution tests: surface consistent deconvolution **(a)**, surface consistent spectral whitening **(b)**, single trace deconvolution **(c)**, spectral whitening **(d)**. Inlets in each panel shows spectral content of the gather. Simple spectral whitening

time. This procedure significantly boosts the amplitudes below 300 ms for both deep reflections and much stronger surface waves. Because our data set consist of large offsets it was possible to simply mute the surface waves with hand-picked tail mutes, and use only wide angle reflections for imaging. As presented in Fig. 8, a clear deep reflection at c.a. 550 ms is visible for times preceding the arrival of the surface waves. Moreover, this strong reflection was visible at a number of shots and for various frequencies. Spectral whitening in the range of 10–180 Hz was applied further on to minimise the effects of variable geophones

d results in the sharpest wide-angle reflections. All panels presented with AGC (100 ms), front mute and high-pass filter (> 30 Hz) applied

and source plate coupling, and some source generated noise. Unfortunately, standard velocity analysis using semblance plots was not possible for deep structure because of lack of deep reflections between 200 and 600 ms. For stack we used extrapolated velocities as in Fig. 6. The effect of normal moveout and stack is presented in Fig. 9. The main features are the gaps at the deployment contact points. They are the effect of application of tail mutes presented in Fig. 8. This step significantly improves the quality of section, especially at the larger times. Thanks to large offsets for the profile we could simply mute all

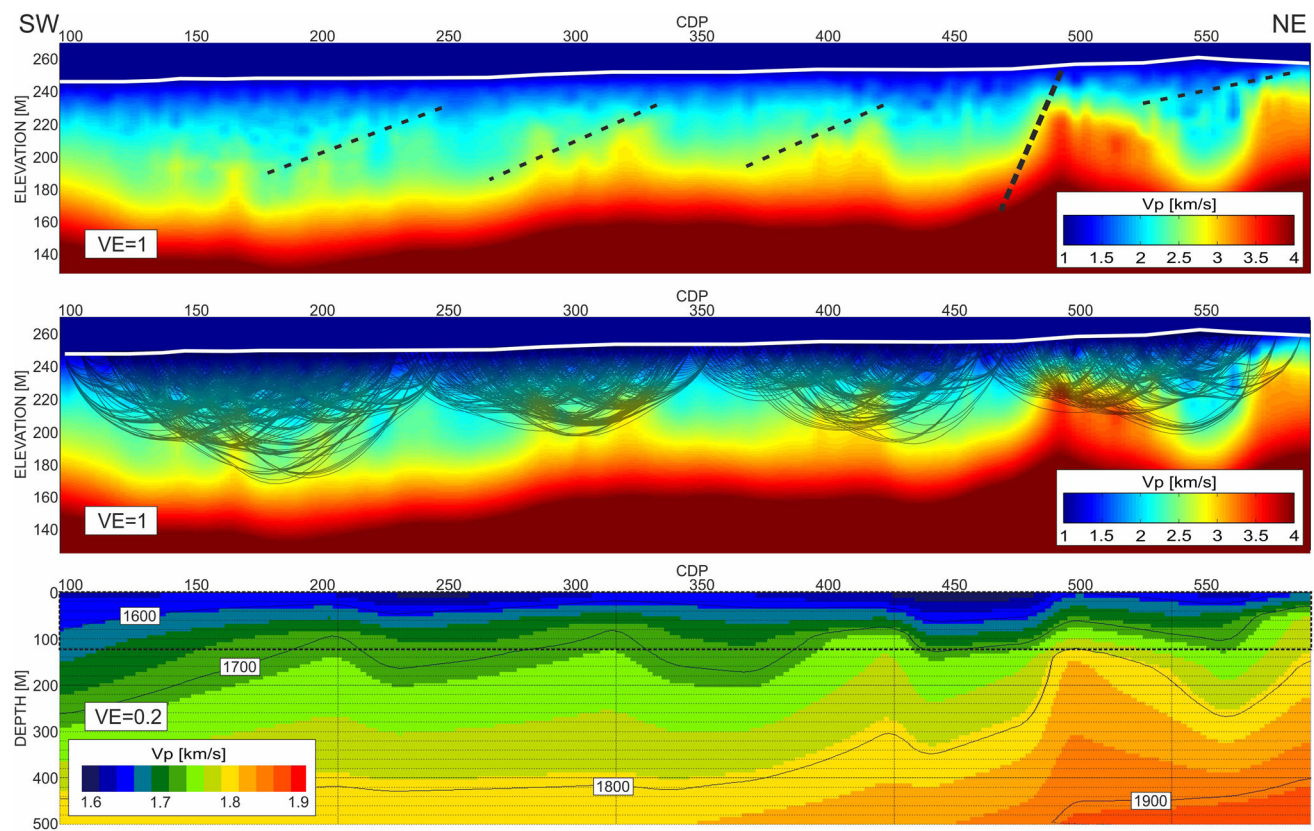


Fig. 6 Result of the first breaks travel time tomography showing the P wave velocity in the shallow structure (top). White line marks the elevation, black dashed lines mark strong dipping velocity gradients indicating the discontinuity of velocities. The middle panels shows the same result with seismic ray paths to mark the well recovered

arrivals related to the surface waves and still recover wide-angle reflection. One important aspect in the processing was correct order of tail mutes, AGC and filters application. It is important to filter the data first then apply tail mute procedure. The other order result in strong filter artefacts below the tail mute times being enhanced by AGC procedure giving strong, artificial reflections at large times. The result of correct processing focused on the deep structures shows clear NE deepening reflection marked with a red line (Fig. 9) at depths from 450 to 700 m.

Conclusions

Shallow seismic investigations yielded detailed images of the Carpathian Foredeep marginal zone. A large offset survey combined with modified accelerated weight drop source was specially designed to allow both high resolution reflection image and refraction tomography. Four strokes of the source give enough energy to observe refractions at all offsets up to 350 m, but also to recognize a deep structure down to 700 m. Two processing paths were used

areas. The lower panel, with different vertical exaggeration ($VE = 0.2$) shows the velocity field based on tomographic result and the velocity analysis, that was further used to the depth conversion. Dashed rectangle marks the area with tomographic velocities

to enhance both shallow and deep structures, resulting in detailed image of the near-surface faults, but also a sharp deep reflection. The 5-m spacing used for both shots and receivers was not dense enough to clearly recognize the first 30 m. Additional information like ERT experiment or different seismic processing, e.g., MASW (Park et al. 1999), and finally joint interpretation might be used to further verify this part of the structure. Still, a clear image of a main fault in the area was presented. This weight drop seismic profile was performed to recognize near-surface structures, that is why it was surprising to observe clear reflection at 700 m (Fig. 9). For surveys of this type with limited number of stations we suggest to use different spacing for shots and receivers. For example deploying stations with 8 m spacing and shooting with 2 m spacing will result in similar fold, but would limit number of deployments, limiting number of repeated shots. Thanks to dense shooting it would be possible to recover shallower structures, but wider deployments would give important long offset refracted arrivals. In the end acquisition time should be similar with higher resolution results. To make it optimal it would be beneficial to perform test shooting and

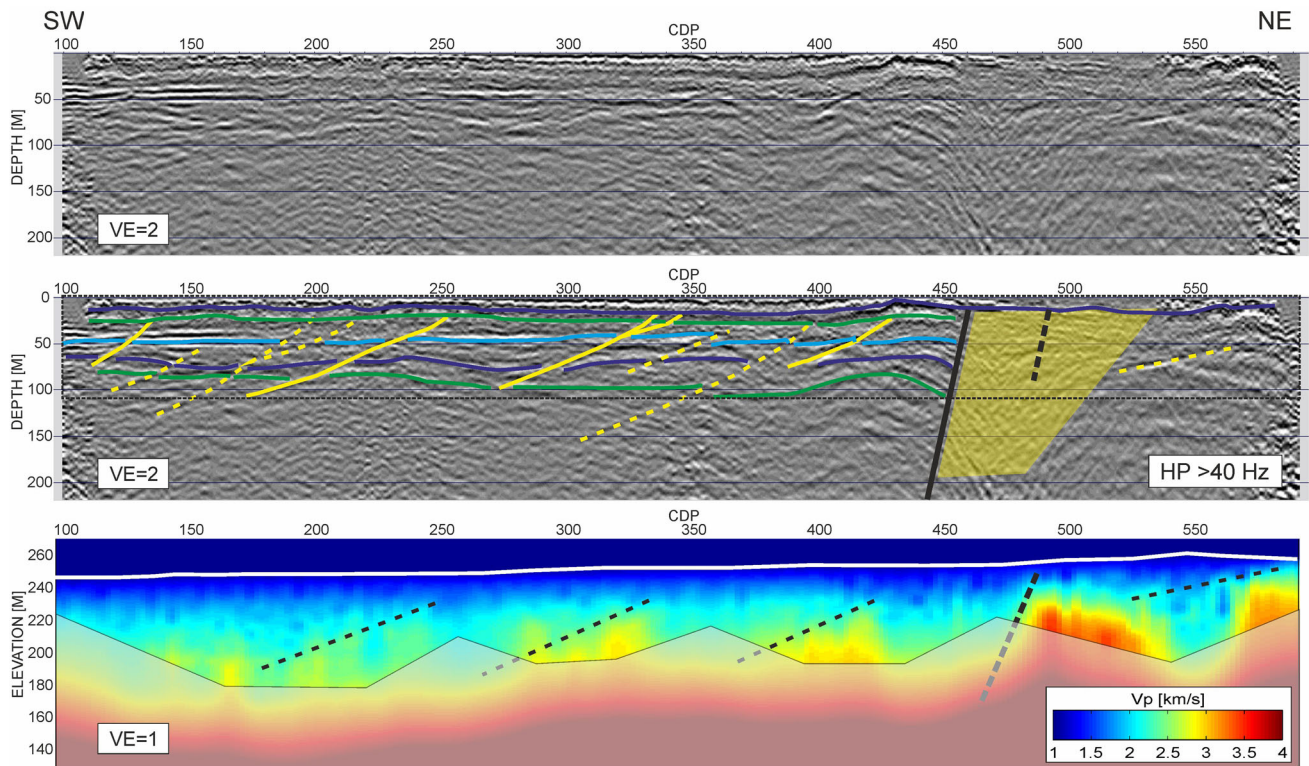


Fig. 7 Shallow structure in the depth domain obtained with shallow reflections enhanced processing (top). The middle panel shows several discontinuities in the flat reflections (marked with colour solid lines) that do not reach the surface. Those marked with solid yellow lines are confirmed with tomography. Yellow polygon marks the area of the low reflectivity that differs from surrounding structures, and

corresponds to a zone of the strong velocity gradient in tomography. Dashed rectangular marks the area as in the lower panel. The lower panel, with different vertical exaggeration (VE = 1), shows tomographic result as in Fig. 6 with an unreliable greyed area without ray coverage

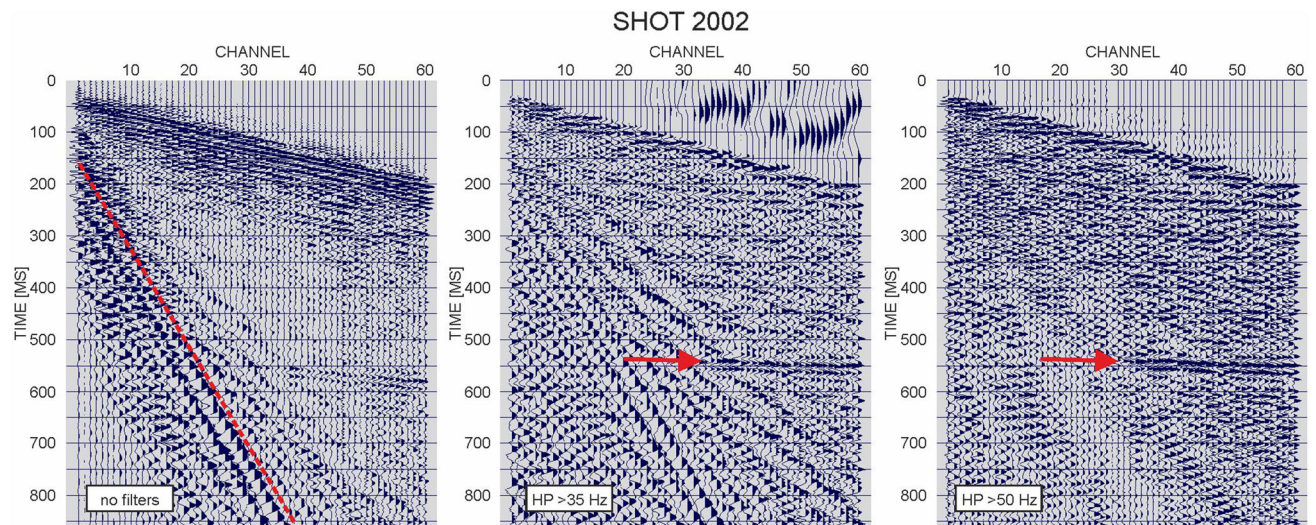


Fig. 8 Clear deep reflection (red arrow) at about 550 ms is visible at a number of shots. Example for shot 2002 shows raw data after diversity stack (left), application of front mute and high pass filter above 35 Hz (middle), and NMO with velocity of 1500 m/s and high pass filter above 50 Hz. Simple high pass filtration clearly removes

surface waves and enhance reflections. Flattening of reflection for small NMO velocity shows deepening of the reflector toward NE. All panels presented with AGC (100 ms) applied. The red line marks the tail mute

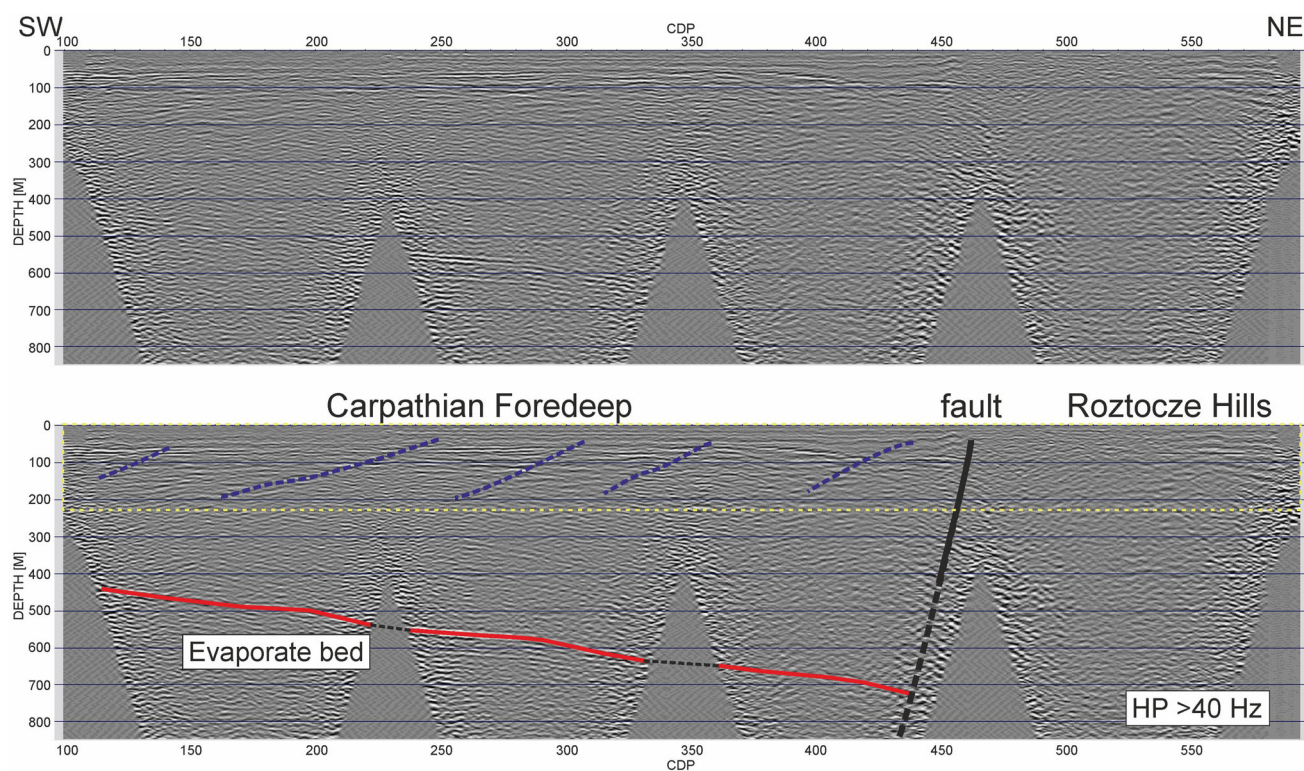


Fig. 9 Time domain stack with deep reflection enhanced processing. The data gaps at the deployment contact points are the effect of tail mute application to remove effect of surface waves. Clear deepening reflection at 450–700 ms marked with red line is visible along the

profile. In shallow part between 50 and 200 ms several discontinuities of reflections are visible. Strong cut-of layering marked with black line is showing the Marginal Zone of the Carpathian Foredeep. Yellow rectangle marks the shallow area as in Fig. 7

recognize the maximum offset of clear observations, and design the survey for specific environment.

The horizon marked in red in Fig. 9 refers to the evaporate layers that occurs throughout the area of the Carpathian Foredeep and represents the best reference horizon for geophysical and geological research in this area. Such a evaporate layer is observed and well documented at much shallower depths in Ukraine.

Summarizing, we show that presented type of seismic survey with weight drop source and standalone stations can lead to a clear image of the structure from 30 down to 700 m, that could be performed effectively with low costs. The key to achieve detailed result is a careful data analysis using multiple techniques, that we hope to improve even further in the future.

Acknowledgements We would like to thank colleagues in the Imaging Department of IG PAS, as well as Editor Michał Malinowski for many suggestions that significantly improved the quality of this paper. This research was funded by National Science Centre, Poland (NCN) Grant UMO-2015/19/B/ST10/01833. Part of this work was supported within statutory activities no. 3841/E-41/S/2017 of the Ministry of Science and Higher Education of Poland.

Open Access This article is distributed under the terms of the Creative Commons Attribution 4.0 International License (<http://creativecommons.org/licenses/by/4.0/>), which permits unrestricted use, distribution, and reproduction in any medium, provided you give appropriate credit to the original author(s) and the source, provide a link to the Creative Commons license, and indicate if changes were made.

References

- Babel M (2004) Badenian evaporite basin of the northern Carpathian Foredeep as a drawdown salina basin. *Acta Geol Pol* 54(3):313–337
- Bachrach R, Nur A (1998) High-resolution shallow seismic experiments in sand, part I: water table, fluid flow and saturation. *Geophysics* 63(1):1225–1233. <https://doi.org/10.1190/1.1444423>
- Bruno PP, Improta L, Castiello A, Villani F, Montone P (2010) The Vallo di Diano fault system: new evidence for an active range-bounding fault in Southern Italy using shallow, high-resolution seismic profiling. *Bull Seismol Soc Am* 100(2):882–890
- Bruno PP, Castiello A, Villani F, Improta L (2013) High-resolution densely spaced wide-aperture seismic profiling as a tool to aid seismic hazard assessment of fault-bounded intramontane basins: application to Vallo di Diano, Southern Italy. *Bull Seismol Soc Am* 103(3):1969–1980
- Buker F, Green AG, Horstmeyer H (1998) Shallow seismic reflection study of a glaciated valley. *Geophysics* 63:1395–1407

- Dusar M, Rijpens J, Sintubin M, Wouters L (2001) Plio-Pleistocene fault pattern of the Feldbiss fault system (southern border of the Roer Valley Graben, Belgium) based on high resolution reflection seismic data. *Neth J Geosci* 80:79–93
- Feroci M, Orlando L, Balia E, Bosman C, Cardarelli E, Deidda G (2000) Some considerations on shallow seismic reflection surveys. *J Appl Geophys* 45:127–139
- Francese RG, Hajnal Z, Schmitt D, Zaja A (2007) High resolution seismic reflection imaging of complex stratigraphic features in shallow aquifers. *Memorie Descrittive della Carta Geologica d'Italia*, LXXVI, pp 175–192
- Green AG, Campbell FM, Kaiser AE, Dorn C, Carpentier S, Doetsch JA, Horstmeyer H, Nobes D, Campbell J, Finnemore M, Jongens R, Ghisetti F, Gorman AR, Langridge RM, McClymont AF (2010) International Conference on Environmental and Engineering Geophysics, p 15
- Hobro JWD (1999) Three-dimensional tomographic inversion of combined reflection and refraction seismic travel-time data. Ph.D. Thesis, Department of Earth Sciences, University of Cambridge, Cambridge, UK
- Jankowski L, Margielewski W (2015) Pozycja tektoniczna Roztocza w świetle historii rozwoju zapadliska przedkarpackiego. *Biuletyn Państwowego Instytutu Geologicznego* 462:7–28
- Jaroszewski W (1977) Synsedymencyjne przejawy miocenijskiej ruchliwości tektonicznej na Roztoczu Środkowym. *Przegląd Geologiczny* 25(8/9):418–427
- Kondracki J (1994) *Geografia Polski, mezoregiony fizyczno-geograficzne*, PWN
- Krzywiec P (2001) Contrasting tectonic and sedimentary history of the central and eastern parts of the Polish Carpathian Foredeep basin—results of seismic data interpretation. *Mar Pet Geol* 18:13–38
- Kurkowski S (1998) Szczegółowa Mapa Geologiczna Polski 1:50 000, arkusz Józefów. Państwowy Instytut Geologiczny
- Majdański M, Trzeciak M, Gaczyński E, Maksym A (2016) Seismic velocity estimation from post-critical wide-angle reflections in layered structures. *Stud Geophys Geod* 60:565–582
- Malinowski M, Guterch A, Narkiewicz M, Probulski J, Maksym A, Majdański M, Środa P, Czuba W, Gaczyński E, Grad M, Janik T, Jankowski L, Adamczyk A (2013) Deep seismic reflection profile in Central Europe reveals complex pattern of Paleozoic and Alpine accretion at the East European Craton margin. *Geophys Res Lett* 40:1–6
- Myśliwiec M (2004) Miocenijskie skały zbiornikowe zapadliska przedkarpackiego. *Przegląd Geologiczny* 52:581–592
- Park CB, Miller RD, Xia J (1999) Multichannel analysis of surface waves. *Geophysics* 64:800–808
- Pullan S, Hunter JA (1990) Delineation of buried bedrock valleys using the optimum offset shallow seismic reflection technique. In: Ward SH (ed) *Geotechnical and environmental geophysics*, vol. 3, Society of Exploration Geophysicists, no 5, pp 75–88
- Robertsson JOA, Holliger K, Green AG, Pugin A, De Iaco R (1996) Effects of near-surface waveguides on shallow high resolution seismic refraction and reflection data. *Geophys Res Lett* 23:495–498
- Roniewicz P, Wysocka A (1999) Charakterystyka sedimentologiczna utworów środkowomiocenijskich północno-wschodniej, brzeżnej strefy zapadliska przedkarpackiego. *Prace Państwowego Instytutu Geologicznego*, CLXVIII, pp 83–97
- Steeple DW (2000) A review of shallow seismic methods. *Ann Geofis* 43:1021–1030
- Steeple DW, Miller RD (1990) Seismic reflection methods applied to engineering, environmental, and groundwater problems. In: Ward SW (ed) *Geotechnical and environmental geophysics*, vol 3, Society of Exploration Geophysicists, no 5, pp 1–30
- Steeple DW, Miller RD (1998) Avoiding pitfalls in shallow seismic reflection surveys. *Geophysics* 63:1213–1224
- Sugiyama Y, Mizuno K, Nanayama F, Sugai T, Yokota H, Hosoya T, Miura K, Takemura K, Kitada N (2003) Study of blind thrust faults underlying Tokyo and Osaka urban areas using a combination of high-resolution seismic reflection profiling and continuous coring. *Ann Geophys* 46:1071–1085
- Vesnaver AL, Gohm G, Madrussani G, Petersen SA, Rossi G (1999) Tomographic imaging by reflected and refracted arrivals at the North Sea. *Geophysics* 64:1862–1952
- Wysocka A (2006) Klastyczne utwory badeńskie Roztocza—przebieg sedymentacji w północnej marginalnej strefie basenu zapadliska przedkarpackiego. *Przegląd Geologiczny* 54:430–437
- Wysocka A, Jasionowski M (2006) Polish part of Roztocze Hills. *POKOS Materiały Konferencyjne* 11–14
- Wysocka A, Krzywiec P, Maksym A (2006) Kamieniołom Józefów. *POKOS Materiały Konferencyjne* 19–24
- Wysocka A, Radwański A, Górka M, Babel M, Radwańska U, Złotnik M (2016) The middle miocene of the fore-Carpathian Basin (Poland, Ukraine and Moldova). *Acta Geol Pol* 66:351–401
- Zelt CA (1999) Modelling strategies and model assessment for wide-angle seismic traveltimes data. *Geophys J Int* 139:183–204